Structural and superconducting properties of $La_{2-x}Sr_xCuO_4$ as a function of Sr content

P. G. Radaelli
Science and Technology Center for Superconductivity, Argonne National Laboratory, Argonne, Illinois 60439

D. G. Hinks and A. W. Mitchell
Materials Science Division, Argonne National Laboratory, Argonne, Illinois 60439

B. A. Hunter and J. L. Wagner
Science and Technology Center for Superconductivity, Argonne National Laboratory, Argonne, Illinois 60439

B. Dabrowski
Materials Science Division, Argonne National Laboratory, Argonne, Illinois 60439
and Department of Physics, Northern Illinois University, Dekalb, Illinois 60115

K. G. Vandervoort, H. K. Viswanathan, and J. D. Jorgensen
Materials Science Division, Argonne National Laboratory, Argonne, Illinois 60439
(Received 3 September 1993)

We have studied the structural and superconducting properties of $La_{2-x}Sr_xCuO_4$ by neutron and x-ray powder diffraction, thermogravimetry, ac susceptibility, and dc magnetization. The kinetics of the synthesis reaction were studied in order to determine the optimum conditions for preparing single-phase samples. The room-temperature and low-temperature structural properties, as determined by neutron powder diffraction, are discussed in detail. By comparing the results of the neutron-diffraction and magnetic measurements, we conclude that superconductivity exists in both the orthorhombic and tetragonal phases. The thermodynamic conditions for the stability of the $La_{2-x}Sr_xCuO_4$ phase are also investigated.

I. INTRODUCTION

$La_{2-x}Sr_xCuO_4$ is the only copper-oxide superconductor for which the chemical composition can be varied over a wide enough range to obtain the full spectrum of electronic properties. With increasing Sr content, the compound evolves from an antiferromagnetic insulator to a superconductor, with a maximum T_c occurring at an "optimum" composition, $x \approx 0.15$, and then to a normal metal.[1] Such behavior, which most other copper-oxide superconductors display over limited ranges, is thought to reflect a universal property of the CuO_2 layers.[2-5] The common feature is the existence of an optimum chemical composition, i.e., optimum hole concentration, at which the maximum T_c is achieved, with T_c decreasing in both the underdoped and overdoped regions. However, many compounds do not display the full range of behavior because either the overdoped or underdoped regions cannot be accessed due to chemical instabilities. For example, it is difficult to overdope $YBa_2Cu_3O_{6+x}$ (Ref. 6) or to underdope $Tl_2Ba_2CuO_{6+x}$ (Ref. 7) by significant amounts. For this reason, $La_{2-x}Sr_xCuO_4$ remains one of the most heavily studied systems. The decrease of T_c and eventual disappearance of superconductivity in the "overdoped" composition range ($x > 0.15$), resulting in normal metallic behavior, is of particular interest. It is critical to establish whether such behavior is intrinsic for these compounds or whether some simpler explanation, such as the effects of increasing defect concentrations, a structural phase transition, or chemical phase separation can explain the suppression of superconductivity. Such explanations have been proposed by some authors, but later disputed by others.

One of the earliest proposals was that the decreasing T_c for $x > 0.15$ resulted from the formation of oxygen vacancies in the CuO_2 plane.[8] Neutron-diffraction measurements had shown that vacancy formation began around $x = 0.15-0.20$, with the vacancy concentration increasing sharply with increasing Sr content. However, Torrance and co-workers[1,9,10] showed that T_c decreased in the same way even for samples in which the oxygen-vacancy concentrations had been reduced by annealing in high oxygen pressures. Annealing the samples at high oxygen pressures shifted the point at which oxygen vacancies first appeared to higher Sr concentrations, but the maximum T_c remained at $x = 0.15$ for all samples. These experiments were responsible for calling attention to the unusual behavior of oxide superconductors in the overdoped composition range.

Chemical inhomogeneity, for Sr concentrations greater than 0.15, was also proposed as a possible explanation. Studies based on different synthesis techniques suggested that the nature of the chemical inhomogeneity depended on the synthesis conditions. For example, samples formed at 1020 °C and cooled slowly in oxygen tended to show $La_2SrCu_2O_6$ as an impurity phase coexisting with

$La_{1.85}Sr_{0.15}CuO_4$ in samples with starting compositions of $x > 0.15$.[8] It was found that the formation of $La_2SrCu_2O_6$ as an impurity phase could be minimized by the use of higher synthesis temperatures. A different kind of two-phase behavior, involving two phases with the $La_{2-x}Sr_xCuO_4$ structure, but with different Sr concentrations (one of the phases having $x \approx 0.15$ and $T_c \approx 35$ K and the other having $x \approx 0.5$) was also reported.[11] Although other synthesis routes yielded samples for which two-phase behavior was not apparent, these observations suggested that $La_{2-x}Sr_xCuO_4$ may be intrinsically unstable for $x > 0.15$. Since the length scale for superconductivity in these compounds is very short, it was speculated that chemical inhomogeneity even on a length scale too short to be observed by conventional diffraction experiments (for example, in the early stages of decomposition) would be responsible for the decrease in T_c.

More recently, at least two groups[12–14] have published results for samples that are judged to be chemically homogeneous by the absence of impurity peaks or peak broadening in x-ray-diffraction data and the sharpness of superconducting transitions. Both groups concluded that chemical inhomogeneity, or phase separation, was not the cause of the decreasing T_c for $x > 0.15$. Based on an abrupt decrease in the Meissner signal at the orthorhombic-to-tetragonal (*O-T*) structural transition, which occurs at $x = 0.21$ at low temperature, Takagi *et al.*[12] concluded that the structural phase transition was responsible for the loss of superconductivity. They argued that the observation of some superconductivity for $x > 0.21$ resulted from local structural inhomogeneity. In similar experiments, Kitazawa and co-workers[13,14] did not see any discontinuity in the Meissner signal at the structural phase transition ($x = 0.21$) and concluded that bulk superconductivity exists in both the orthorhombic and tetragonal phases. They proposed that the abrupt drop in the Meissner signal for $x > 0.21$ observed by Takagi *et al.* was the result of stronger flux-pinning effects in this region rather than a reduced superconducting fraction.

Recently, Yamada and Ido published a careful study on the effect of pressure on both the structural and superconducting properties of $La_{2-x}Sr_xCuO_4$.[15] Their work shows that the application of pressure moves the *O-T* phase transition line to lower strontium concentrations. For example, at 20 kbars, samples with $x = 0.15$ are tetragonal at 20 K. For samples that are orthorhmobic at ambient pressure, the orthorhombicity *decreases* as a function of increasing pressure, while the superconducting critical temperature *increases,* reaching its maximum value at the *O-T* phase transition. In the tetragonal phase, T_c is essentially pressure independent. At 20 kbars, the shape of the T_c vs x curve is very similar to that at ambient pressure: The maximum T_c is reached for $x \approx 0.15$ (~ 42 K), and superconductivity disappears for $x > 0.23$. This study indicates that the proximity of the low-temperature *O-T* line and the disappearance of superconductivity is essentially coincidental, and can be removed by the application of pressure. In addition, it suggests that optimal superconducting properties are attained in the tetragonal phase, while the orthorhombic distortion may actually depress T_c.

In light of the controversy that still exists concerning the properties of $La_{2-x}Sr_xCuO_4$ as a function of Sr content, we present here the results of an extensive study of the superconducting and structural properties for the composition range $0.00 \leq x \leq 0.375$. We report a simple method for making single-phase samples and discuss the criteria for assessing the chemical homogeneity on the appropriate length scales. The structural properties, as determined by neutron powder diffraction, are discussed in considerable detail. In agreement with Kitazawa *et al.*,[13] we conclude that bulk superconductivity exists in both the orthorhombic and tetragonal phases. Thus, we find no alternative explanation for why T_c decreases in the overdoped composition region. We discuss briefly the synthesis conditions for which multiphase samples are obtained and speculate concerning how such phenomena have contributed to misleading conclusions in the literature.

II. SYNTHESIS AND CHARACTERIZATION OF SAMPLE QUALITY

A detailed analysis of the correlation between structural and physical properties in solid solution compounds, such as $La_{2-x}Sr_xCuO_4$, requires samples with a high degree of chemical homogeneity. In the case of high-temperature superconducting cuprates, samples must be homogeneous at the level of the superconducting coherence length (10–100 Å). Therefore, coherent compositional fluctuations with short wavelength, such as those produced by spinodal decomposition, could have profound effects on the superconducting properties. X-ray or neutron Bragg diffraction, due to the intrinsic coherence length of several hundred angstroms, would be insensitive to this type of local segregation phenomena.

In the case of $La_{2-x}Sr_xCuO_4$, the relatively weak dependence of lattice constants on composition, particularly in the tetragonal phase, makes it impossible to rule out the existence of even macroscopic inhomogeneities. For the present samples in the $x > 0.2$ region, Δx could be as high as 0.03, based solely on the widths of x-ray and neutron Bragg peaks. As we will later show, a far higher degree of homogeneity (at least a factor of 3) is required to address such subtle questions as the existence of superconductivity in the tetragonal phase. Therefore, the observation of sharp Bragg peaks, even in a high-resolution diffraction experiment, does not insure sufficient homogeneity. It is our opinion that the following requirements must be also fulfilled: (a) Samples must be free from nonisostructural impurity phases; in most cases, such phases are in equilibrium with one end of the solid solution, and therefore a concentration gradient is created around each grain of impurity. (b) Optimal thermodynamic synthesis conditions must be chosen to ensure fast reaction kinetics. (c) Magnetic superconducting transitions in low field should be sharp. If combined with a knowledge of the T_c vs x curve, the transition width places an upper limit on the degree of inhomogeneity of the sample. In addition, in the "underdoped" and "overdoped" regions it is essential to ascertain the absence of high-T_c material.

All samples for this study were synthesized by two-step solid-state reaction. High-purity La_2O_3 (Reaction grade 99.99%), $SrCO_3$ (Puratronics grade 99.995%), and CuO (Puratronics grade 99.999%) were weighed in the proper stoichiometric amounts, mixed and ball milled in agate jars under *N*-amyl alcohol for approximately 1 h. After drying, the mixture was isostatically pressed at room temperature into rods, placed in an Al_2O_3 boat, and heated to 700 °C for 24 h under dynamic vacuum. The purpose of this first step was to decompose $SrCO_3$ into SrO and CO_2. The prereacted samples—a mixture of La_2O_3, SrO, Cu_2O, CuO, and a small amount of binary compounds—were then quickly introduced into a hot furnace in air, at the final synthesis temperature. After firing for the appropriate time, the samples were quenched to room temperature by rapidly removing them from the furnace. Quenching ensures, as much as possible, that the chemical and phase composition properties at synthesis temperature are preserved in the final sample. X-ray-diffraction patterns were obtained on a Rigaku diffractometer using Cu K_α radiation. Lattice constants were measured by Rietveld refining the x-ray patterns using the LHPM program,[16] based on the Wiles and Young code.[17]

Reaction kinetics were studied by monitoring the evolution of lattice parameters as a function of reaction time at a given temperature. This study showed that for high-temperature synthesis (i.e., 1170 °C) all samples with $x \leq 0.3$ are synthesized very rapidly ($t \approx 15$ min) directly from the precursors. At lower synthesis temperatures, samples with $x > x_c$ (with x_c being a critical value dependent on the temperature) are synthesized by forming nonisostructural impurity phases, which then slowly decompose to form the desired compound, in addition to the "2:1:4" phase. The strongest impurity peaks can be assigned to the "two-layer" compound ($La_2SrCu_2O_6$). The intensity of the impurity peaks slowly decreases with prolonged annealing.

During this process, the lattice constants of the "2:1:4" phase gradually change. Figure 1 shows the evolution of lattice constants as a function of reaction time for a sample with nominal strontium content $x = 0.3$, for three reaction temperatures 900, 1000, and 1150 °C. The lattice constant evolution is consistent with a slow incorporation of strontium into the "2:1:4" phase. A comparison with the structural parameters of single-phase samples (see Sec. IV), indicates that for synthesis at 1000 °C, the strontium content of the "2:1:4" phase is initially as low as $x \approx 0.2$.

The average lattice constants asymptotically approach the values measured on single-phase samples, indicating that, even for low-temperature synthesis, no macroscopic phase separation occurs. However, the kinetic history of samples synthesized at low temperature makes it extremely likely that small amounts of strontium-deficient material may persist, even after long annealings. Such inhomogeneities have profound effects on the superconducting properties, while remaining virtually undetectable by diffraction.

In Fig. 2 the ac susceptibility curves of three powdered samples, all with nominal composition $x = 0.3$ but with different thermal history, are compared (for the details of the magnetic measurements, see Sec. III). Sample 1 was reacted for 408 h at 900 °C in air, without intermediate grindings, followed by rapid quenching to room temperature. Sample 2 was reacted for 128 h at 1150 °C in air, without intermediate grindings, followed by rapid quenching to room temperature. Sample 3 was reacted for 24 h at 1170 °C in air, followed by rapid quenching to room temperature. The three samples have almost identical lattice constants ($a \approx 3.765$ Å, $c \approx 13.25$ Å), and display equally sharp Bragg peaks, but their shielding fractions differ by a factor of 50, due to the presence of residual amounts of strontium-deficient material. For sample 3, prolonged annealings at 700 °C in pure oxygen did not increase the diamagnetic fraction, indicating that oxygen deficiency is not the cause of the difference in superconducting properties between the three samples. We

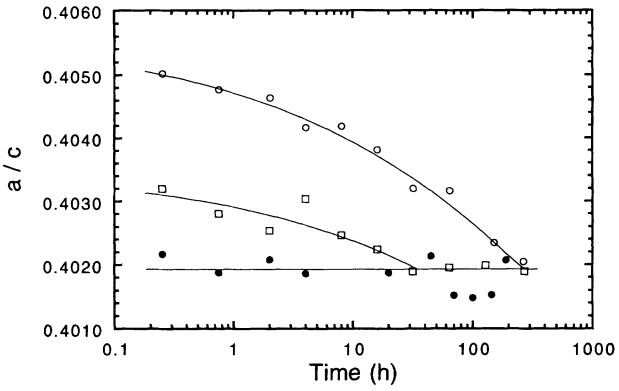

FIG. 1. Room-temperature a/c ratios versus reaction time for samples reacted in air at 900 °C (open circles), 1000 °C (squares), and 1150 °C (closed circles), followed by rapid quenching to room temperature. The lines are guides for the eye.

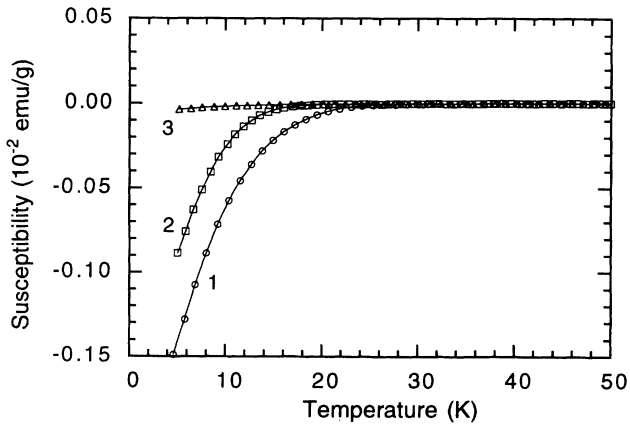

FIG. 2. ac susceptibility vs temperatures for samples with nominal composition $x = 0.3$, measured in a 1-G ac field at 100 Hz. Sample 1 (circles) was reacted for 408 h at 900 °C in air, followed by rapid quenching to room temperature. Sample 2 (squares) was reacted for 128 h at 1150 °C in air followed by rapid quenching to room temperature. Sample 3 (triangles) was reacted for 24 h at 1170 °C in air, followed by rapid quenching to room temperature.

therefore conclude that solid-state reaction produces the most homogeneous samples when synthesis is carried out close to the melting point, followed by rapid quenching to room temperature.

A series of samples with variable strontium content ($0 \leq x \leq 0.3$) was synthesized for further characterization of the structural and superconducting properties. The previously described two-step solid-state reaction method was employed, using a synthesis temperature of 1170 °C in air, followed by rapid quenching to room temperature. The reaction time was approximately 24 h. Each sample (approximately 25 g of material) was split into three parts (*A*, *B*, and *C*). *A* samples were studied in the *as made* state. *B* samples were annealed at 700 °C in flowing oxygen, followed by slow cooling to room temperature. For selected compositions, *C* samples were annealed at 1100 °C in 0.6 kbar oxygen pressure, using a hot isostatic press externally heated apparatus, followed by slow cooling to room temperature.

Neutron-powder-diffraction (NPD) data were collected on all *A*- and *B*-type samples, and on selected *C*-type samples, at various temperatures, using the special environment powder diffractometer [18](SEPD) at Argonne's Intense Pulsed Neutron Source (IPNS), and analyzed using the Rietveld method.[19] A discussion of the experimental details of the NPD experiments and of the structural properties of these samples, as obtained from analysis of the NPD data, can be found in Sec. IV. However, some of the results will be anticipated here and in Sec. III, as needed.

Neutron-diffraction patterns confirmed that the samples are single phase (i.e., they do not contain any nonisostructural impurity phases), with the peak widths of the "2:1:4" phase being comparable to the instrumental resolution. Neutron-diffraction data for the $x = 0.1875$ compound are shown in Fig. 3, as a representative example.

Figure 4 shows the lattice constant ratio a/c, measured at 295 K, as a function of x for *A* and *B* samples. Lattice constant ratios are almost insensitive to systematic errors, such as the sample position in the neutron beam, which would increase the scattering of the data. *A*- and *B*-type samples have identical a/c ratios, within the error bars, at least up to $x = 0.24$. For higher values of x, the a/c ratio varies for different oxidizing conditions, indicating that oxygen vacancies are present in the as-made samples, and are progressively filled up by oxygen annealing. This interpretation is supported by the results of the thermogravimetric analysis (TGA). The a/c ratio, measured on selected *C*-type samples, was found to be identical to that for *B*-type samples, within the error bars, at least up to $x = 0.3$.

The oxygen content of all samples was measured by TGA, using a Perkin Elmer Series 7 Thermal Analysis system. Weight loss was monitored during reduction of the samples in pure H_2 atmosphere, while heating to 700 °C. Taking into account the small variability in oxygen content, the chemical formula of this series can be written as $La_{2-x}Sr_xCuO_{4-\delta}$, where δ, for all our samples, is a small positive number. In Fig. 5, the oxygen deficiency per formula unit δ is plotted as a function of x for *A*, *B*, and *C* samples. There is a significant amount of

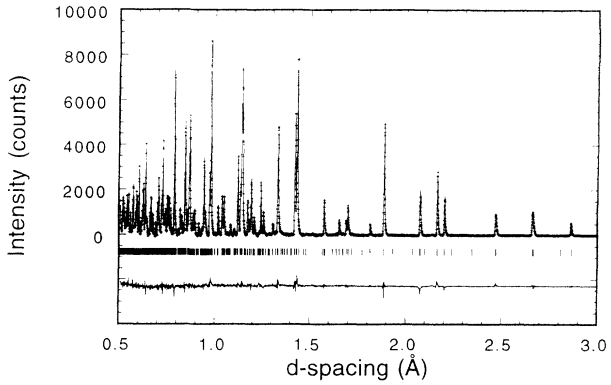

FIG. 3. Rietveld refinement profile for the $x = 0.1875$ *B*-type sample at 10 K. The plus (+) signs are the raw time-of-flight neutron-powder-diffraction data. The solid line is the calculated profile. The background was fit as part of the refinement, but has been subtracted before plotted. Tick marks below the diffraction profile mark the position of allowed Bragg reflections for the Bmab (No. 64) space group. A difference curve (observed minus calculated) is plotted at the bottom.

scatter in the data for the as-made (quenched) samples. This scatter is probably real, since the accuracy of the measurement is about ± 0.01 (as evidenced by the data for $x < 0.2$), and may result from the difficulty of perfectly reproducing the quenching process. However, it is clear that oxygen vacancies are not formed in significant numbers until strontium concentrations beyond $x = 0.2$ are reached. For samples annealed in 1 atm of oxygen or in high-pressure oxygen, these oxygen vacancies are filled for strontium concentrations less than about 0.3. Thus, the TGA results are in agreement with the conclusions about oxygen vacancies that were drawn from the variation of the c/a ratio with x (Fig. 4). As we will discuss later, bulk superconductivity occurs in the region $0.05 \leq x \leq 0.24$. Annealing in 1 atm of oxygen at 700 °C is adequate to fill oxygen vacancies over this composition range. We conclude that oxygen vacancies are not responsible for the decrease of T_c in the overdoped region.

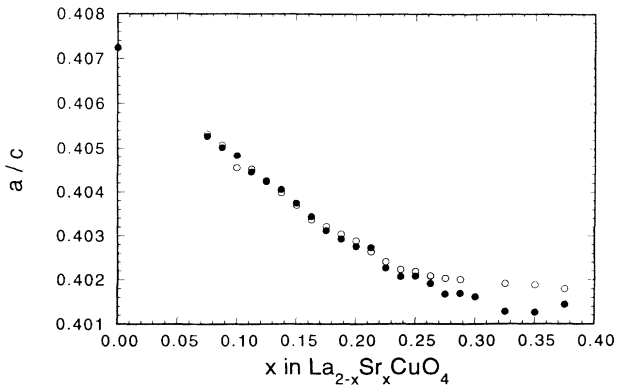

FIG. 4. a/c ratio vs x at 10 K, as obtained from neutron powder-diffraction data, for as-made *A*-type samples (open circles), and oxygen annealed *B*-type samples (closed circles).

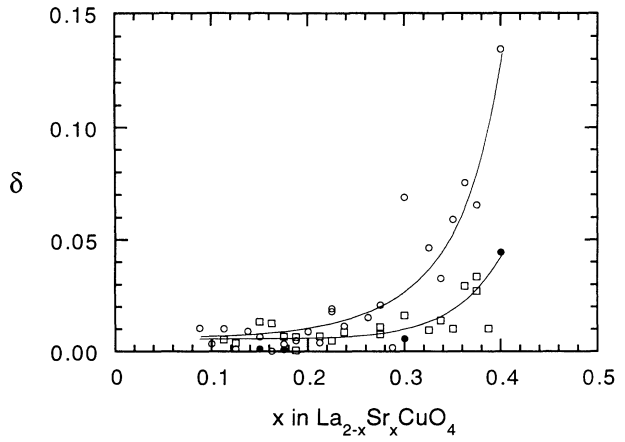

FIG. 5. Oxygen deficiency per formula unit δ (as in $La_{2-x}Sr_xCuO_{4-\delta}$), versus x, for as-made A-type samples (open circles), 1 atm oxygen-annealed B-type samples (squares), and high-pressure oxygen annealed C-type samples (closed circles). The lines are guides for the eye. The accuracy of the measurement is approximately ± 0.01.

Moreover, since the number of oxygen vacancies is very small even for the as-made (quenched) samples for $x < 0.24$, we are unable to probe the effect of oxygen vacancies on superconductivity in these experiments.

III. SUPERCONDUCTING PROPERTIES

In order to address the relevant questions regarding the superconducting properties versus strontium concentration, we must determine both the superconducting transition temperatures and the superconducting phase fraction. It is particularly important to learn whether bulk superconductivity is present in the tetragonal phase.

Magnetic techniques cannot be used to unambiguously measure the superconducting phase fraction (i.e., the amount of superconducting material in a sample) without knowledge of the sample's internal topology (i.e., the distribution of voids and nonsuperconducting regions within the sample), and, in the case of field-cooled magnetization, of the flux-pinning behavior. Specific-heat measurements do not suffer such limitations, but superconducting phase fractions cannot be directly calculated from specific-heat anomalies without a knowledge of the basic mechanism of superconductivity, which is at present lacking for the cuprates. Even abrupt changes of the strength of the specific-heat anomaly cannot be immediately associated with a change in superconducting phase fraction. For example, in the case of oxygen-deficient $YBa_2Cu_3O_{6+x}$ it has been shown that dramatic changes in strength of the specific-heat anomaly occur with small departure from optimum doping, without any change in Meissner or shielding signals.[20]

Despite these difficulties, the following statements can be made: (a) If corrected for demagnetization effects, the Meissner fraction (i.e., the field-cooled diamagnetic fraction) always *underestimates* the true superconducting phase fraction, due to flux pinning, flux trapping, and penetration length effects. Therefore, a high Meissner fraction always guarantees bulk superconductivity. However, a low Meissner fraction does not necessarily imply a small amount of superconducting phase. (b) If corrected for penetration length effects, the shielding fraction (i.e., the zero-field-cooled diamagnetic fraction) always *overestimates* the true superconducting phase fraction, due to the screening of voids and nonsuperconducting regions in the sample. Therefore, the knowledge of both shielding and Meissner fractions provides a useful way of bracketing the superconducting phase fraction. Since the bracket is always wider for a sintered sample than for a powder sample, due to the more complex topological nature of the former, measurements should always be performed on powder samples.

Ac susceptibility measurements (to determine the shielding fraction) were performed on warming on finely ground samples using a Lake Shore Cryotronics ac susceptometer, in a 1-G field at 100 Hz. Low-field dc magnetization measurements (to determine the Meissner fraction) were performed in a 1-G field on cooling in the field-cooled (FC) mode, using a low-field superconducting quantum interference device (SQUID) magnetometer. Diamagnetic fractions are reported in units of emu/g, and are calculated by dividing the measured magnetic moment by the sample weight, without applying any demagnetization correction. For comparison, the "ideal" diamagnetic fraction of a sample of density ρ, expressed in emu/g, is given by $\chi_{\text{ideal}} = -1/4\pi\rho$. For powder samples, which are constituted of disconnected crystallites, ρ can be taken as the theoretical density ($\rho = M_W \times N_A / V$), where M_W is the molecular weight, N_A is Avogadro's number, and V is the unit-cell volume, as measured by neutron diffraction (see Sec. IV). For the samples of the present study, χ_{ideal} varies between -1.11×10^{-2} for $x=0$ and -1.13×10^{-2} for $x=0.3$, and, for all practical purposes, can be approximated by a straight line in between. The uncorrected shielding fraction of a powder sample can exceed the ideal value (typically by less than 20%), due to demagnetization effects and to some intergranular coupling. For each sample, both the onset and the midpoint critical temperatures are reported. The midpoint T_c is defined as the temperature at which the magnetic moment is half the value at 5 K.

As already mentioned, A-, B-, and C-type samples have nearly identical superconducting properties. This can be explained by the small oxygen variability in the range of composition where bulk superconductivity is observed. As we already discussed, a small amount of oxygen vacancies, at the limit of TGA sensitivity, cannot be ruled out, especially for A-type samples. However, even if they are present, oxygen vacancies have evidently very little effect on the superconducting properties in such small concentrations. For this reason, we will focus attention primarily on the samples annealed in 1 atm of oxygen (B-type samples).

Figure 6 shows the shielding fractions (as determined by ac susceptibility) and the Meissner fractions (as determined by SQUID magnetization) versus x for B-type samples. The position of the O-T phase transition line at low temperature, as determined by neutron powder diffraction (see Sec. IV), is also indicated. Based on these

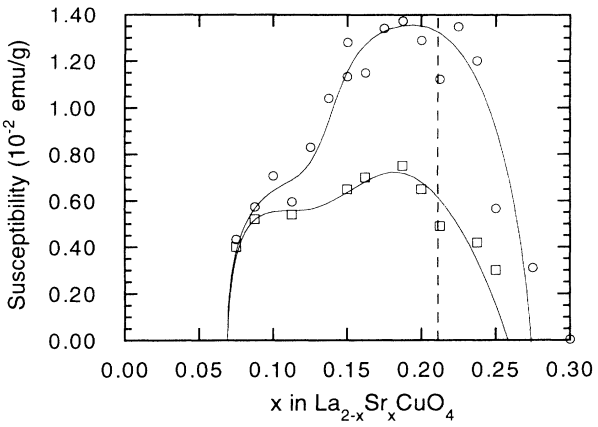

FIG. 6. ac diamagnetic phase fraction (circles) and Meissner fraction (squares) at 5 K, vs x. Solid lines are guides to the eye. The dotted line indicates the position of the *O-T* phase line as determined from low-temperature neutron powder diffraction.

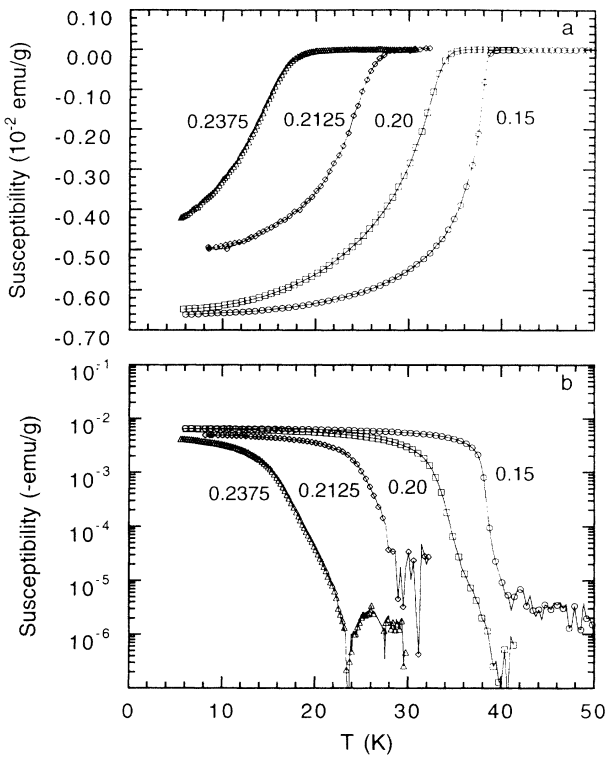

FIG. 7. FC magnetization vs temperature for samples with $x=0.15$ (circles), $x=0.20$ (squares), 0.2125 (rhombi), and 0.2375 (triangles), plotted on a linear scale (a) and on a logarithmic scale (b). The logarithmic scale emphasized the behavior close to the transition temperature. The instrumental noise level ($\sim 10^{-6}$ emu/g) is shown above the transition for comparison.

results, the following observations can be made: (a) The shielding fraction *increases* with increasing x up to $x=0.15$, probably due to the decrease of the superconducting penetration length. As already noticed by Kitazawa *et al.* and Nagano *et al.*[13,14] the $x=0.1125$ sample has a somewhat anomalously low value of the shielding fraction. At this same composition, a structural anomaly and the disappearance of superconductivity are observed in the $La_{2-x}Ba_xCuO_4$ system.[21,22] For $0.15 \leq x \leq 0.2375$ the shielding fraction is greater than the "ideal" value, with some sample-to-sample fluctuations. This indicates that the superconducting penetration length is, at this point, much smaller than the average grain size. The shielding fraction suddenly drops for $x > 0.2375$. (b) The Meissner fraction, for all measured samples, varies between 35 and 65 %, indicating that all samples are bulk superconductors. (c) The ratio between Meissner and shielding fractions decreases with increasing x (from $>90\%$ for $x=0.075$ to $\sim 30\%$ for $x=0.2375$), indicating that flux-pinning effects become stronger. We conclude that, for all samples with $0.075 \leq x \leq 0.25$, a large part of the material is in the superconducting state below the critical temperature. A study performed by Nagano *et al.*,[14] in which the effect of penetration length and flux pinning are carefully examined, has concluded that the true superconducting phase fraction of similar powder samples in this composition range is close to 100%. The reduced shielding fraction for our $x=0.25$ sample suggests that this composition is on the borderline of the superconducting region.

It is clear from Fig. 6 that at least three samples (in the range $0.21 \leq x \leq 0.24$) with tetragonal crystal structure are bulk superconductors, according to our definition. To explore the issue of superconductivity in the tetragonal structure in further detail it is useful to plot the Meissner data on a logarithmic scale, so that small amounts of superconductivity can be seen. The Meissner susceptibility versus temperature curves for the $x=0.15$, $x=0.20$, $x=0.2125$, and $x=0.2375$ samples are plotted in Fig. 7 on a linear scale (a) and on a logarithmic scale (b). The $x=0.2375$ sample, well within the tetragonal region, has a well-defined onset around 18 K, and a high Meissner fraction ($\sim 40\%$ of the ideal value). In addition, there is no indication in the data of a diamagnetic signal above 22 K. The measurement is sensitive at least to 0.02% superconducting phase fraction. At 18 K, the Meissner fraction of this sample is $\leq 2\times 10^{-4}$ emu/g [Fig. 7(b)]. On the other hand, for the $x=0.2125$ sample, over 80% of the transition is completed at 18 K. As a consequence, tetragonal material is responsible for at least 70% of the Meissner transition observed in the $x=0.2375$ sample. We therefore conclude that bulk superconductivity extends to compositions that have the tetragonal crystal structure at low temperature, i.e., superconductivity in this composition region does not result from compositional inhomogeneity. In addition, we observed no significant discontinuity in the diamagnetic fractions at the *O-T* phase boundary. The presence of considerable sample-to-sample variations ($\sim 1.5\times 10^{-3}$ emu/g for the shielding fractions and $\sim 1\times 10^{-3}$ emu/g for the Meissner fractions) would prevent us from seeing a small discontinuity, but there is certainly no discontinuity of the magnitude reported by Takagi *et al.*[12]

In Fig. 8 the ac onset and midpoint critical temperatures of samples that display bulk superconductivity are plotted versus x. The position of the *O-T* transition line, as determined from neutron powder diffraction, is also shown. The T_c versus x curve displays a plateau around

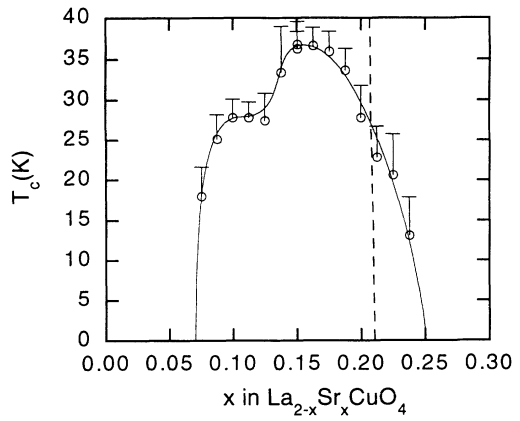

FIG. 8. Onset (top of the error bars) and midpoint (open circles) critical temperatures versus x, from ac susceptibility measurements. The solid line is a guide to the eye. The dotted line indicates the position of the O-T phase line as determined from low-temperature neutron powder diffraction.

$x=0.12$, as already reported in the literature.[13–15,23] T_c reaches a maximum around $x=0.15$, and then rapidly decreases. No discontinuity in the T_c versus x curve is observed at the O-T phase boundary. In light of this observation and of the discussion of the previous section, we therefore conclude that the O-T phase boundary has no effect on the superconducting properties of $La_{2-x}Sr_xCuO_4$.

IV. STRUCTURAL PROPERTIES

Neutron-powder-diffraction (NPD) data were collected on all samples at 10, 70, and 295 K, using the special environment powder diffractometer[18] (SEPD) at Argonne's Intense Pulsed Neutron Source (IPNS). For low-temperature data collection, samples were contained in indium-sealed, thin-walled vanadium cans 1 cm in diameter, filled with helium exchange gas.

The powder-diffraction data were analyzed with the Rietveld technique, using the IPNS time-of-flight Rietveld code.[19] Only data from the backscattering detector banks ($2\theta=145°$) were used in the refinements.

Only results from the B samples (oxygen annealed) will be discussed. As we already mentioned, the structural parameters of A, B, and C samples are essentially identical up to $x\approx0.24$, which is the region of interest as far as superconductivity is concerned.

The lattice parameters and atomic coordinates of B samples at 10, 70, and 295 K, as obtained from Rietveld refinement of NPD, are reported in Tables I, II, and III, respectively. At constant temperature, the Debye-Waller factors B do not show any systematic variation as a function of x. Therefore, for the sake of brevity, they are not reported for every sample. For every temperature, the Debye-Waller factors averaged over all the strontium concentrations are listed in Table IV.

The structural phase diagram of $La_{2-x}Sr_xCuO_4$ contains, at least up to $x\approx0.375$, only two crystallographic phases: the high-temperature tetragonal (HTT) and the

TABLE I. Lattice parameters and atomic coordinates at 10 K for $La_{2-x}Sr_xCuO_4$ oxygen-annealed B-type samples. The nonstandard space groups Bmab (isomorphic to the standard Cmca, No. 64) and $F4/mmm$ (isomorphic to the standard $I4/mmm$, No. 139) were used for the orthorhombic and tetragonal phases, respectively. Numbers in parentheses are statistical errors of the last significant digit. The atomic positions are La/Sr [0,y,z], Cu[0,0,0], O(1)[1/4,1/4,z], O(2)[0,y,z]. The occupancy of all atoms was set to the full value. Isotropic Debye-Waller temperature factors were refined for each data set, but since they do not show any systematic dependence on x, only the average values are reported in Table IV.

x	a (Å)	b (Å)	c (Å)	y(La/Sr)	z(La/Sr)	z[O(1)]	y[O(2)]	z[O(2)]	R_{wp}/R_{exp}
0.0000	5.3346(1)	5.4148(1)	13.1172(1)	−0.0083(2)	0.3616(1)	−0.0084(1)	0.0404(2)	0.1837(1)	6.213/3.016
0.0750	5.3269(1)	5.3819(1)	13.1640(1)	−0.0074(2)	0.3611(1)	−0.0068(1)	0.0332(2)	0.1835(1)	5.210/3.499
0.0875	5.3260(1)	5.3763(1)	13.1672(1)	−0.0067(2)	0.3610(1)	−0.0065(1)	0.0318(2)	0.1831(1)	6.324/4.427
0.1000	5.3241(1)	5.3706(1)	13.1700(1)	−0.0063(2)	0.3610(1)	−0.0065(1)	0.0304(2)	0.1829(1)	5.541/2.628
0.1125	5.3246(1)	5.3627(1)	13.1813(1)	−0.0061(2)	0.3609(1)	−0.0057(2)	0.0282(3)	0.1829(1)	5.950/4.035
0.1250	5.3241(1)	5.3585(1)	13.1859(1)	−0.0056(2)	0.3609(1)	−0.0055(2)	0.0267(3)	0.1828(1)	6.332/4.343
0.1375	5.3231(1)	5.3542(1)	13.1881(1)	−0.0061(2)	0.3609(1)	−0.0051(2)	0.0261(3)	0.1827(1)	4.868/2.517
0.1500	5.3247(1)	5.3486(1)	13.1973(1)	−0.0052(3)	0.3607(1)	−0.0045(2)	0.0237(4)	0.1827(1)	7.182/4.855
0.1625	5.3247(1)	5.3437(1)	13.2057(1)	−0.0043(3)	0.3608(1)	−0.0042(2)	0.0214(4)	0.1824(1)	5.429/3.489
0.1750	5.3228(1)	5.3349(1)	13.2076(1)	−0.0038(4)	0.3607(1)	−0.0027(4)	0.0181(5)	0.1824(1)	6.437/4.230
0.1875	5.3221(1)	5.3313(1)	13.2098(1)	−0.0049(5)	0.3606(1)	−0.0027(4)	0.0154(7)	0.1820(1)	6.252/4.355
0.2000	5.3200(1)	5.3261(1)	13.2146(1)	−0.0025(5)	0.3605(1)	−0.0022(3)	0.0114(7)	0.1819(1)	6.486/3.986
0.2125	5.3238(1)		13.2150(1)	0.0	0.3608(1)	0.0	0.0	0.1815(1)	7.304/5.233
0.2250	5.3199(1)		13.2219(1)	0.0	0.3606(1)	0.0	0.0	0.1813(1)	6.372/4.018
0.2375	5.3197(1)		13.2266(1)	0.0	0.3606(1)	0.0	0.0	0.1813(1)	5.515/3.445
0.2500	5.3177(1)		13.2214(1)	0.0	0.3602(1)	0.0	0.0	0.1813(1)	5.502/2.939
0.2625	5.3193(1)		13.2282(1)	0.0	0.3603(1)	0.0	0.0	0.1809(1)	5.906/3.078
0.2750	5.3143(1)		13.2257(1)	0.0	0.3603(1)	0.0	0.0	0.1809(1)	5.672/2.635
0.2875	5.3138(1)		13.2236(1)	0.0	0.3601(1)	0.0	0.0	0.1809(1)	5.187/2.917
0.3000	5.3119(1)		13.2275(1)	0.0	0.3600(1)	0.0	0.0	0.1807(1)	6.130/4.064
0.3500	5.3113(1)		13.2310(1)	0.0	0.3600(1)	0.0	0.0	0.1800(1)	5.584/3.418
0.3750	5.3097(1)		13.2212(1)	0.0	0.3599(1)	0.0	0.0	0.1797(1)	4.577/2.743

TABLE II. Lattice parameters and atomic coordinates at 70 K for $La_{2-x}Sr_xCuO_4$ oxygen-annealed *B*-type samples. The space-group conventions and general atomic positions are the same used in Table I.

x	a (Å)	b (Å)	c (Å)	y(La/Sr)	z(La/Sr)	z[O(1)]	y[O(2)]	z[O(2)]	R_{wp}/R_{exp}
0.0750	5.3289(1)	5.3809(1)	13.1650(1)	−0.0071(2)	0.3611(1)	−0.0064(2)	0.0328(2)	0.1834(1)	5.525/4.064
0.0875	5.3279(1)	5.3754(1)	13.1692(1)	−0.0064(3)	0.3611(1)	−0.0063(2)	0.0318(3)	0.1832(1)	7.372/5.762
0.1000	5.3261(1)	5.3695(1)	13.1717(1)	−0.0063(2)	0.3610(1)	−0.0064(1)	0.0299(2)	0.1830(1)	5.509/2.630
0.1125	5.3265(1)	5.3618(1)	13.1831(1)	−0.0056(3)	0.3608(1)	−0.0058(2)	0.0278(3)	0.1830(1)	7.352/5.722
0.1250	5.3261(1)	5.3575(1)	13.1876(1)	−0.0057(3)	0.3608(1)	−0.0054(2)	0.0260(4)	0.1830(1)	7.570/5.881
0.1375	5.3251(1)	5.3534(1)	13.1902(1)	−0.0060(2)	0.3608(1)	−0.0047(2)	0.0254(3)	0.1827(1)	4.835/2.612
0.1500	5.3266(1)	5.3476(1)	13.1992(1)	−0.0053(4)	0.3608(1)	−0.0041(3)	0.0226(5)	0.1826(1)	7.686/5.575
0.1625	5.3267(1)	5.3427(1)	13.2075(1)	−0.0038(3)	0.3607(1)	−0.0038(2)	0.0210(4)	0.1824(1)	5.596/3.859
0.1750	5.3247(1)	5.3342(1)	13.2095(1)	−0.0033(5)	0.3607(1)	−0.0030(4)	0.0154(7)	0.1822(1)	7.236/5.244
0.1875	5.3237(1)	5.3305(1)	13.2116(1)	−0.0044(6)	0.3607(1)	−0.0018(5)	0.0137(8)	0.1819(1)	5.721/3.336
0.2000	5.3212(1)	5.3261(1)	13.2162(1)	−0.0020(7)	0.3605(1)	−0.0013(5)	0.0082(10)	0.1818(1)	6.500/4.006
0.2125	5.3245(1)		13.2160(1)	0.0	0.3608(1)	0.0	0.0	0.1815(1)	7.785/5.677
0.2250	5.3210(1)		13.2231(1)	0.0	0.3607(1)	0.0	0.0	0.1813(1)	8.043/6.333
0.2375	5.3208(1)		13.2283(1)	0.0	0.3605(1)	0.0	0.0	0.1813(1)	6.303/4.614
0.2500	5.3186(1)		13.2229(1)	0.0	0.3602(1)	0.0	0.0	0.1813(1)	5.444/3.010
0.2625	5.3198(1)		13.2291(1)	0.0	0.3603(1)	0.0	0.0	0.1808(1)	6.198/3.571
0.2750	5.3152(1)		13.2274(1)	0.0	0.3602(1)	0.0	0.0	0.1809(1)	6.092/3.426
0.2875	5.3147(1)		13.2253(1)	0.0	0.3601(1)	0.0	0.0	0.1810(1)	5.442/3.672
0.3000	5.3127(1)		13.2293(1)	0.0	0.3600(1)	0.0	0.0	0.1807(1)	6.202/4.099
0.3500	5.3120(1)		13.2321(1)	0.0	0.3600(1)	0.0	0.0	0.1801(1)	6.103/4.003
0.3750	5.3105(1)		13.2227(1)	0.0	0.3598(1)	0.0	0.0	0.1797(1)	4.859/3.120

low-temperature orthorhombic (LTO). The HTT and LTO structures are schematically shown in Fig. 9.

According to the standard conventions, the HTT and LTO phases have space group symmetry $I4/mmm$ (No. 139) and *Cmca* (No. 64), respectively. However, in order to use a consistent set of axes throughout the phase diagram, it is convenient to resort to nonstandard space-group settings for both phases. Therefore, in the remainder of the paper, all structural data will be reported using the $F4/mmm$ space-group setting for the HTT phase and the Bmab space-group setting for the LTO phase. According to these conventions, the c axis is always the longest axis (~ 13.2 Å). The a axis in the tetragonal phase is approximately equal to $(a+b)/2$ in

TABLE III. Lattice parameters and atomic coordinates at 295 K for $La_{2-x}Sr_xCuO_4$ oxygen-annealed *B*-type samples. The space-group conventions and general atomic positions are the same used in Table I.

x	a (Å)	b (Å)	c (Å)	y (La/Sr)	z(La/Sr)	z[O(1)]	y[O(2)]	z[O(2)]	R_{wp}/R_{exp}
0.0000	5.3574(1)	5.4005(1)	13.1555(1)	−0.0063(2)	0.3613(1)	−0.0076(1)	0.0343(2)	0.1840(1)	6.002/3.181
0.0750	5.3508(1)	5.3664(1)	13.2030(1)	−0.0031(3)	0.3610(1)	−0.0057(2)	0.0233(4)	0.1831(1)	5.333/3.452
0.0875	5.3492(1)	5.3588(1)	13.2076(1)	−0.0041(5)	0.3609(1)	−0.0058(2)	0.0197(6)	0.1829(1)	6.275/3.586
0.1000	5.3489(2)	5.3543(2)	13.2126(1)	−0.0014(4)	0.3609(1)	−0.0046(2)	0.0160(5)	0.1829(1)	6.505/3.300
0.1125	5.3471(1)		13.2205(1)	0.0	0.3609(1)	0.0	0.0	0.1826(1)	5.870/3.453
0.1250	5.3466(1)		13.2266(1)	0.0	0.3611(1)	0.0	0.0	0.1825(1)	5.941/3.151
0.1375	5.3449(1)		13.2281(1)	0.0	0.3610(1)	0.0	0.0	0.1825(1)	6.320/3.601
0.1500	5.3422(1)		14.2317(1)	0.0	0.3608(1)	0.0	0.0	0.1824(1)	6.184/3.757
0.1625	5.3401(1)		13.2364(1)	0.0	0.3609(1)	0.0	0.0	0.1823(1)	6.811/4.502
0.1750	5.3381(1)		13.2420(1)	0.0	0.3609(1)	0.0	0.0	0.1821(1)	7.502/4.552
0.1875	5.3371(1)		13.2458(1)	0.0	0.3607(1)	0.0	0.0	0.1822(1)	5.274/3.220
0.2000	5.3353(1)		13.2469(1)	0.0	0.3607(1)	0.0	0.0	0.1819(1)	5.849/3.567
0.2125	5.3330(1)		13.2419(1)	0.0	0.3608(1)	0.0	0.0	0.1820(2)	4.372/2.677
0.2250	5.3316(1)		13.2538(1)	0.0	0.3605(1)	0.0	0.0	0.1818(1)	7.148/4.973
0.2375	5.3304(1)		14.2572(1)	0.0	0.3603(1)	0.0	0.0	0.1816(1)	5.173/3.306
0.2500	5.3292(1)		14.2539(1)	0.0	0.3600(1)	0.0	0.0	0.1816(1)	5.756/4.146
0.2625	5.3286(1)		14.2581(1)	0.0	0.3601(1)	0.0	0.0	0.1813(1)	5.457/3.391
0.2750	5.3279(1)		13.2642(1)	0.0	0.3600(1)	0.0	0.0	0.1813(1)	6.850/4.837
0.2875	5.3260(1)		13.2591(1)	0.0	0.3599(1)	0.0	0.0	0.1811(1)	5.618/3.751
0.3000	5.3251(1)		13.2591(1)	0.0	0.3599(1)	0.0	0.0	0.1809(1)	6.096/4.058
0.3250	5.3226(1)		13.2639(1)	0.0	0.3598(1)	0.0	0.0	0.1809(1)	6.731/4.938
0.3500	5.3218(1)		13.2628(1)	0.0	0.3597(1)	0.0	0.0	0.1805(1)	5.288/3.251
0.3750	5.3220(1)		13.2572(1)	0.0	0.3598(1)	0.0	0.0	0.1802(1)	4.817/3.325

TABLE IV. Isotropic Debye-Waller temperature factors averaged over all the samples at 10, 70, and 295 K. Numbers in parentheses are standard deviations from the average values. The temperature factors do not show any systematic variation as a function of x.

Atom	Thermal parameter B (Å^2) at 10 K	Thermal parameter B (Å^2) at 70 K	Thermal parameter B (Å^2) at 295 K
La/Sr	0.11(8)	0.13(7)	0.38(10)
Cu	0.07(8)	0.08(7)	0.26(8)
O1	0.21(7)	0.23(8)	0.50(12)
O2	0.55(9)	0.60(9)	1.13(7)

the orthorhombic phase ($\sim$5.35 Å). In the orthorhombic phase, the "tilt" axis (i.e., the axis perpendicular to the mirror plane) coincides with the a axis.

The reduction of symmetry from tetragonal to orthorhombic in the low-temperature, low-doping region of the phase diagram reflects the response of the system to a bond-length mismatch between the LaO and the CuO_2 layers. The mismatch can be quantified by means of the so-called Goldsmidt tolerance factor $t=(\text{La-O})/\sqrt{2}(\text{Cu-O})$,[24] where La-O and Cu-O are the "preferred" bond lengths as obtained from standard ionic or covalent radii.[25] For undoped La_2CuO_4 at room temperature, $t=0.87$, indicating that the CuO_2 layers are under compression, while the LaO layers are under tension. The mismatch between the two layers decreases as a function of x, due to the removal of electrons from antibonding orbitals, and as a function of temperature. The latter effect is predominantly due to the increase of the equilibrium La-O bond length as a function of temperature. When $t<1$, a reduction of symmetry from tetragonal to orthorhombic allows the strain to be partially relieved. This is accomplished in two ways: (a) O(1) is moved off the Cu plane, increasing the Cu-O(1) distance; and (b) the four in-plane La-O(2) bond lengths are made unequal. Figure 10 shows the La-O bond lengths as a function of x at 10, 70, and 295 K. For $x=0$ at 10 K, the difference between the two bond lengths along the b axis is as large as 0.5 Å, making La effectively eightfold coordinated. The movement of O(2) in the b direction is by far the largest internal distortion in this system, and provides the driving force for the phase transition. However, it is only indirectly responsible for the development of spontaneous strain in the orthorhombic phase. The orthorhombic strain arises from a departure of the O(1)-Cu-O(1) "scissors" angle from 90°, which allows, for a given Cu-O(1) distance, a shorter La-O bond length *in the a direction.*

The (a) and (b) distortions result in a cooperative "tilt" of the CuO_6 octahedra, where the Cu-O(2) vector remains roughly (but not exactly) perpendicular to the plane defined by the Cu-O(1) vectors. However, the tilt is *not* rigid, since the scissors angle departs from 90°. In fact, in the case of a rigid tilt of the octahedra, one would predict $a>b$, while the opposite is always observed (Fig. 11). In the orthorhombic phase, we can define two independent tilt angles (θ_1 and θ_2), based on y[O(2)] and z[O(1)], respectively. The difference θ_1-θ_2 measures the departure of the Cu-O(2) vector from being perpendicular to the plane defined by the Cu-O(1) vectors. Experimentally, the values of θ_1 and θ_2 are found to be very close to each other.

The Cu-O(1) bond length as a function of x at 10, 70, and 295 K is shown in Fig. 12. Due to the number of degrees of freedom, in the orthorhombic phase the Cu-O(1) and the La-O(2) in-plane distances are independent. The figure shows that, in the orthorhombic phase, the Cu-O(1) distance is temperature independent, presumably reflecting the amount of doping on the CuO_2 planes. The increased number of constraints in the tetragonal phase results in a reduction of the slope of the curves and in the development of a temperature dependence for this bond length.

The structural phase transition in K_2NiF_4-type structures have been extensively analyzed from a group-theoretical point of view (see, for example, Ref. 26, and references cited therein). Several authors studied the

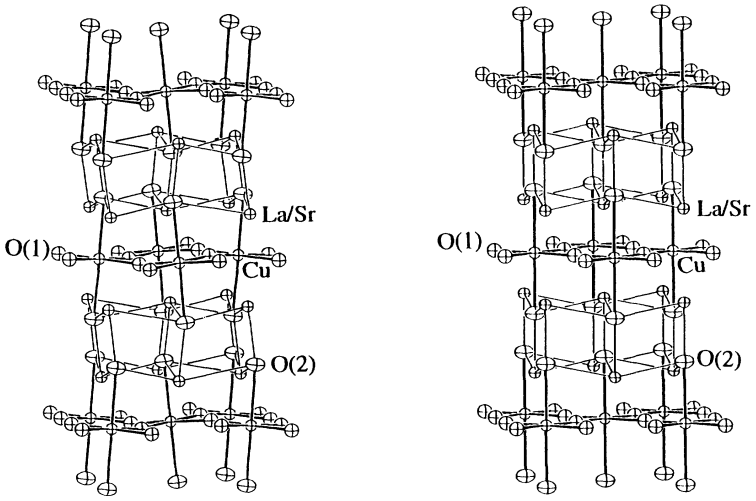

FIG. 9. Structure of the LTO (left) and HTT (right) phases. According to our conventions, the two structures have Bmab and F4/mmm space-group symmetry, respectively. The a axis is perpendicular to the plane of the paper, the b axis is horizontal and the c axis is vertical.

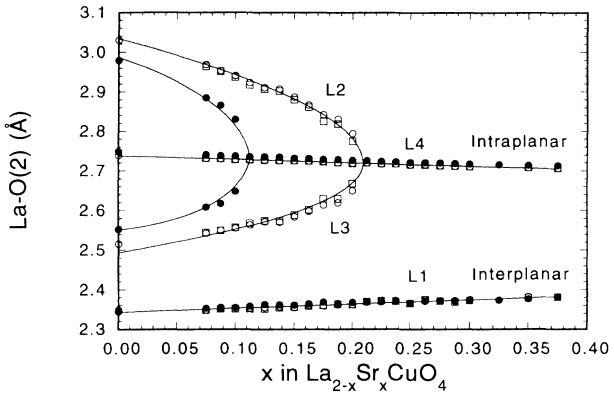

FIG. 10. La-O(2) bond lengths vs x at $T=10$ K (open circles), 70 K (squares), and 295 K (closed circles). The lines are guides to the eye. The La-O(2) distance along the c axis ($L1$) has the smallest value for all samples (2.3–2.4 Å). With increasing x, the two La-O(2) distances along the b axis ($L2$ and $L3$) approach each other and the La-O(2) distance along the a axis ($L4$). In the tetragonal phase, $L2$, $L3$, and $L4$ are equal by symmetry. $L1$ and $L4$ have weak composition and temperature dependence, and show no discontinuity at the phase transition.

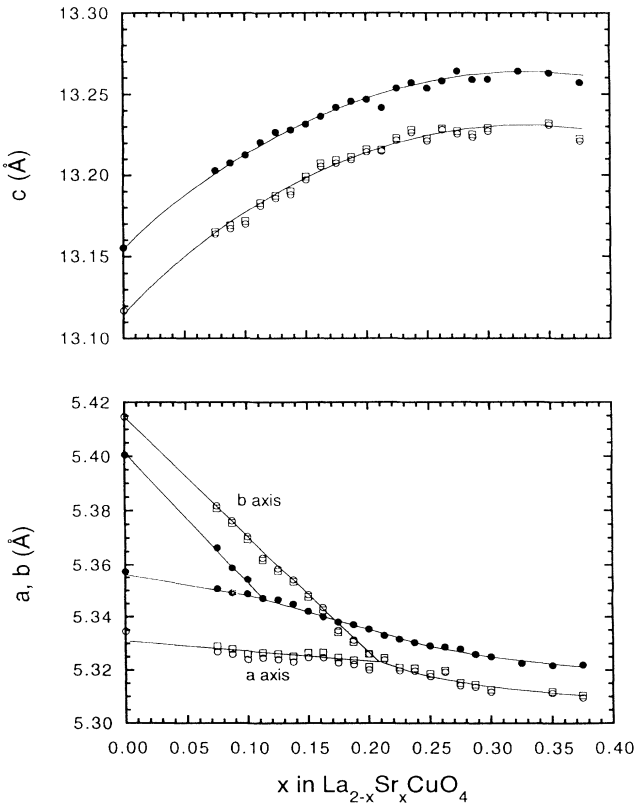

FIG. 11. a,b (bottom), and c (top) vs x at $T=0$ K (open circles), 70 K (squares), and 295 K (closed circles). The lines are guides to the eye.

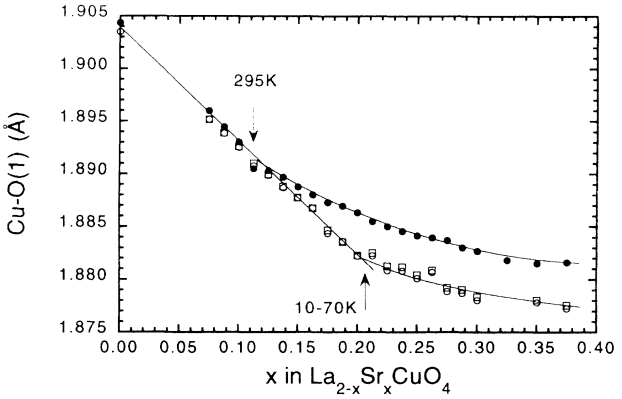

FIG. 12. Cu-O1 bond lengths vs x at $T=10$ K (open circles), 70 K (squares), and 295 K (closed circles). The lines are guides to the eye. The arrows indicate the position of the O-T phase transition at room temperature and at low temperature.

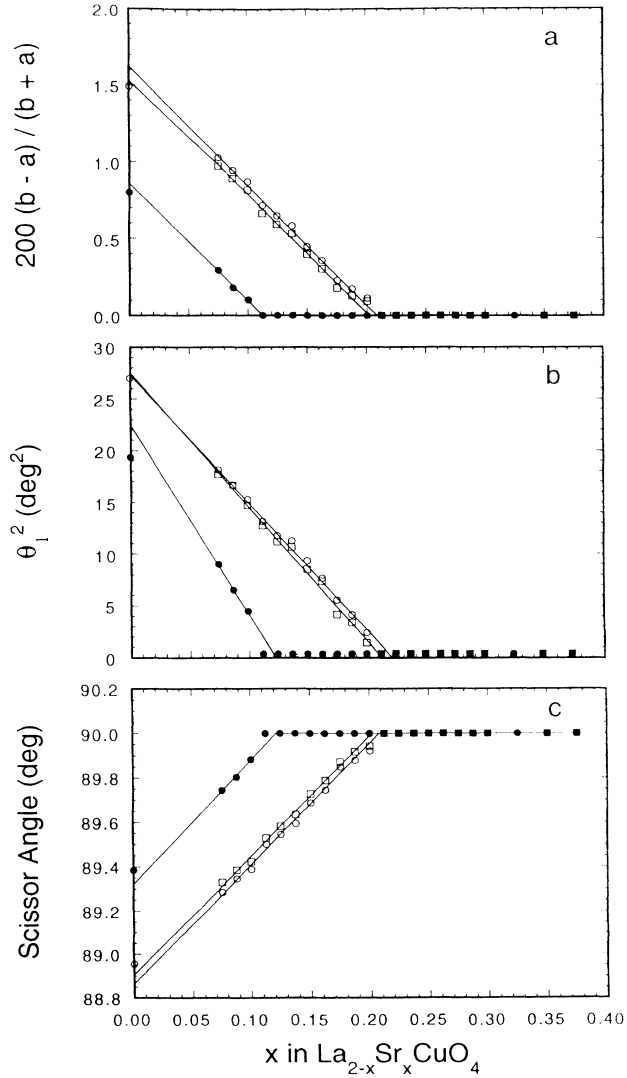

FIG. 13. (a) Orthorhombic strain (b) square of the tilt angle θ_1, defined as $\arctan(y[(O)2]\times b/z[(O)2]\times c)$. (c) "scissors" angle, defined as $2\arcsin(a/4d_{\text{Cu-(O)1}})$ as a function of x at 10 K (open circles), 70 K (squares) and 295 K (closed circles). The lines are best linear fits through the data in the orthorhombic region.

specific case of the $(La,M)_2CuO_4$ compounds (M=Sr, Ba, Ca, Nd, etc.) (Refs. 22 and 27–29) and found that the structural phase diagram of these systems can be described, in the framework of the Landau theory, using a single irreducible representation of the $I4/mmm$ (parent) space group. This representation describes the condensation of soft phonons at the X point on the Brillouin-zone boundary of the tetragonal cell, and is indicated as X_3^+ according to Stokes and Hatch's conventions.[30] The order parameter of X_3^+ is an axial vector, which describes the "tilt" distortion. The direction of the vector coincides with the tilt axis, and its magnitude is proportional to the tilt angle. According to the Landau theory, the $I4/mmm \rightarrow Bmab$ phase transition is allowed (although not required) to be second order. For this phase transition, the order parameter is parallel to the [1,1,0] or $[1,\bar{1},0]$ tetragonal axes.

The expansion of the free energy in powers of the order parameter has been worked out in detail in the previously cited references,[22,27–29] and will not be repeated here. However, for the purpose of comparison with the experimental results, we will describe the predicted behavior of some of the structural parameters as a function of the thermodynamic variables (temperature, pressure, composition, etc.) near the structural phase transition, in the context of mean-field theory. Although mean-field theory does not include the effect of fluctuations, it is expected to be reasonably accurate at low temperature.

(i) The tilt angles are proportional to the magnitude of the order parameter. Therefore, they are zero in the high-symmetry phase ($I4/mmm$), and behave as $(T_{PT}-T)^{1/2}$ or $(x_{PT}-x)^{1/2}$ in the low-symmetry ($Bmab$) phase near the phase transition. All the parameters that are proportional to a tilt angle [like the La-(O)2 distances along the b axis] should behave in the same way.

(ii) The spontaneous strain is quadratically coupled to the order parameter in the Landau free-energy expansion. Therefore it should behave *linearly*, as a function of the thermodynamic parameters, in the low-symmetry phase near the phase transition. The same is true for the O(1)-Cu-O(1) scissors angle.

The orthorhombic strain, the square of the tilt angle θ_1, and the scissors angle as a function of x at 10, 70, and 295 K are shown in Figs. 13(a), 13(b), and 13(c), respectively. It is apparent from the figures that these parameter behave according to mean-field theory throughout almost the entire orthorhombic region, particularly at low temperature. In particular, the linear behavior of the orthorhombic strain allows the critical composition x_{PT} to be determined with great accuracy by extrapolation. The values of x_{PT} obtained in this way are 0.209(2), 0.202(2), and 0.113(4) at 10, 70, and 295 K, respectively. The 10-K value is in excellent agreement with the one reported in Ref. 12.

V. PHASE STABILITY

Considerable attention has been given to the possibility of some form of chemical decomposition or phase separation for $La_{2-x}Sr_xCuO_4$ with strontium contents greater than x=0.15–0.2. Although the nature of the multiphase behavior has been controversial, essentially all authors agree that the difficulty of producing single-phase homogeneous samples increases markedly at strontium concentrations greater than x=0.15–0.2. We previously reported x-ray- and neutron-diffraction evidence for two kinds of impurity phases that are commonly observed for samples in this composition range. $La_2SrCu_2O_6$ (a metallic but nonsuperconducting compound) in combination with $La_{1.85}Sr_{0.15}CuO_4$ is often observed for samples that are fired at temperatures below about 1100 °C and slowly cooled.[8] In samples fired at higher temperatures, the amount of $La_2SrCu_2O_6$ decreased markedly, but we observed a mixture of two $La_{2-x}Sr_xCuO_4$ phases with different strontium contents (one of which was x=0.15).[11] Takagi *et al.*[12] showed that any diffraction evidence for the latter two-phase behavior could be eliminated by annealing for long times (up to one month) at 850–1000 °C. They did not report the abundance of $La_2SrCu_2O_6$ as an impurity phase in their samples. Their hypothesis was that the lack of chemical homogeneity was simply a result of sluggish reaction kinetics for $x>0.15$. For samples with $x \leq 0.15$ the long anneals did not change the properties, while for the high strontium concentrations, the superconducting properties were changed. However, even the samples annealed for long times showed traces of superconductivity with T_c=36–39 K, consistent with the existence of a small amount of material with composition $x \approx 0.15$; i.e., the samples were never perfectly homogeneous. No differences were seen in the diffraction data, consistent with the concept (discussed earlier in this paper) that the superconducting properties are a much more sensitive probe of homogeneity than is diffraction when the concentration of impurity phases is small.

In the present study we have shown that homogeneous samples, with no trace of superconductivity for $x>0.24$, can be made in relatively short times (24 h or less) if high synthesis temperatures (1170 °C) are used and the samples are quenched rather than slowly cooled. As judged by the magnetic properties, samples made in this way are more homogeneous than those annealed for very long times (up to one month) at lower temperatures ($\sim$1000 °C). This result led us to investigate further the phase stability of $La_{2-x}Sr_xCuO_4$ for $x>0.15$. It is important to distinguish between inhomogeneity that results from sluggish reaction kinetics and that which results from intrinsic features of the high-temperature phase diagram. Our own investigation of reaction kinetics (described earlier in this paper) confirms that the diffraction pattern evolves to that consistent with a homogeneous sample after long anneal times at 900–1000 °C. However, measurements of the superconducting properties continue to show the existence of superconductivity at average strontium compositions for which no superconductivity would be present if the samples were truly single phase. Thus, the times required to determine whether perfectly homogeneous samples can be made at these lower temperatures become prohibitively long. Without such experiments, it cannot be confirmed that the difficulty in making homogeneous samples results from sluggish reaction kinetics.

Similar behavior has been reported for the $La_{2-x}Ba_xCuO_4$ system. Yoshimura *et al.* report compositional phase separation for $x > 0.16$ and postulate the existence of a miscibility gap in the phase diagram for temperatures below about 960 °C.[31] However, because of the way their experiments were done, beginning with two-phase mixtures and annealing for long times to attempt to make single-phase samples, they may not be able to differentiate between sluggish reaction kinetics and true thermodynamic phase separation.

We have focused attention on experiments that probe true chemical decomposition or phase separation. One starts with a single-phase homogeneous sample (in the present case, synthesized by quenching from 1170 °C) and investigates changes in the properties when this sample is subsequently annealed at temperatures lower than the synthesis temperature. In such experiments, we consistently observe evidence for decomposition. Figure 14 shows the resistivity data for a sample of composition $x = 0.375$. The as-made sample is metallic, and shows no superconductivity. When this sample is annealed in 20% oxygen for 24 h at 950, 1000, or 1050 °C, a superconducting transition appears, showing that such an anneal promotes decomposition with one of the products being $La_{2-x}Sr_xCuO_4$ with strontium concentrations that are superconducting. Diffraction data for these samples show no changes (i.e., no impurity-phase Bragg peaks or peak broadening) for 24-h anneals, as one would expect for small concentrations of the decomposition products. Similar results are obtained for samples with any strontium concentration greater than $x = 0.15$–0.2, depending on the annealing temperature and oxygen partial pressure. Although we have not fully explored this behavior, these results suggest that $La_{2-x}Sr_xCuO_4$ for $x > 0.15$–0.2 is not chemically stable at temperatures below about 1100 °C. Further studies of this kind will be required to fully understand the high-temperature phase diagram of this material and to learn the stability field of $La_{2-x}Sr_xCuO_4$ as a function of strontium content, temperature, and oxygen partial pressure. Until such work is done in a comprehensive way, the question of chemical stability in the $La_{2-x}Sr_xCuO_4$ for $x > 0.15$–0.2 remains unanswered. However, even if some compositions are metastable (as is not uncommon for copper-oxide superconductors), we have no evidence that the metastability influences the superconducting properties.

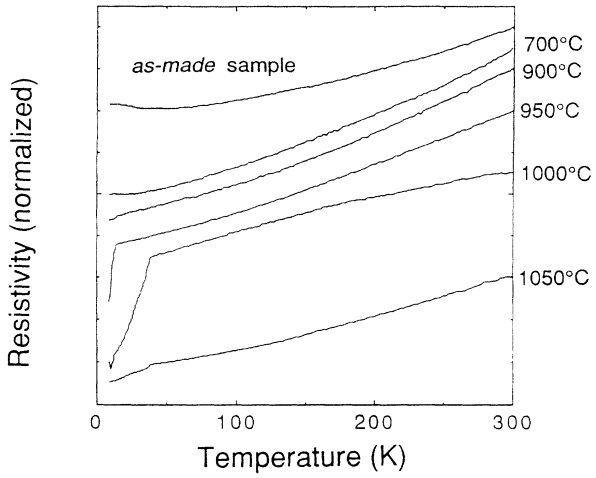

FIG. 14. Normalized resistivity $\rho(T)/\rho(300\ K)$ vs temperature for $La_{2-x}Sr_xCuO_4$ samples with $x = 0.375$. The curves are shifted relative to each other so they do not overlap. The top curve is for an as-made sample (synthesized for 24 h at 1170 K in air, followed by rapid quenching to room temperature). The other curves are for the same sample, after annealing in 20% oxygen at different temperatures. For annealing temperatures between 950 and 1050 °C, a resistive anomaly below 50 K indicates the presence of superconducting material.

ACKNOWLEDGMENTS

This work was supported by the National Science Foundation through the Science and Technology Center for Superconductivity Grant No. DMR 91-20000 (P.G.R., B.A.H., J.L.W., B.D.), and by the US Department of Energy, Basic Energy Sciences-Materials Sciences, under Contract No. W-31-109-ENG-38 (D.G.H., A.W.M., B.D., K.G.V., H.K.V., and J.D.J.).

[1] J. B. Torrance, Y. Tokura, A. I. Nazzal, A. Bezinge, T. C. Huang, and S. S. Parkin, Phys. Rev. Lett. **61**, 1127 (1988).

[2] J. L. Tallon, R. G. Buckley, E. M. Haines, M. R. Presland, A. Mawdsley, N. E. Flower, and J. Loram, Physica C **185-189**, 855 (1991).

[3] Y. J. Uemura, G. M. Luke, B. J. Sternlieb, J. H. Brewer, J. F. Carolan, W. N. Hardy, R. Kadono, J. R. Kempton, R. F. Kiefl, S. R. Kreitzman, P. Mulhern, T. M. Riseman, D. L. Williams, B. X. Yang, S. Uchida, H. Takagi, J. Gopalakrishnan, A. W. Sleight, M. A. Subramanian, C. L. Chien, M. Z. Cieplak, G. Xiao, V. Y. Lee, B. W. Statt, C. E. Stronach, W. J. Kossler, and X. H. Yu, Phys. Rev. Lett. **62**, 2317 (1989).

[4] M.-H. Whangbo, D. B. Kang, and C. C. Torardi, Physica C **158**, 371 (1989).

[5] H. Zhang and H. Sato, Phys. Rev. Lett. **70**, 1697 (1993).

[6] J. L. Tallon and N. E. Flower, Physica C **204**, 237 (1992).

[7] Y. Shimakawa, Y. Kubo, T. Manako, and H. Igarashi, Phys. Rev. B **40**, 11 400 (1989).

[8] D. G. Hinks, B. Dabrowski, K. Zhang, C. U. Segre, J. D. Jorgensen, L. Soderholm, and M. A. Beno, *High-Temperature Superconductors,* edited by M. B. Brodsky, R. C. Dynes, K. Kitazawa, and H. L. Tuller, MRS Symposia Proceedings No. 99 (Materials Research Society, Pittsburgh, PA, 1988), p. 9.

[9] J. B. Torrance, A. Bezinge, A. I. Nazzal, T. C. Huang, S. S. Parkin, D. T. Keane, S. J. LaPlaca, P. M. Horn, and G. A. Held, Phys. Rev. B **40**, 8872 (1989).

[10] C. Marin, J. Y. Henry, and J. X. Boucherle, Solid State Commun. **86**, 425 (1993).

[11] J. D. Jorgensen, P. Lightfoot, S. Pei, B. Dabrowski, D. R. Richards, and D. G. Hinks, in *Advances in Superconductivity-III,* Proceedings of the 3rd International Symposium on Superconductivity, 6–9 November, 1990, Sendai,

Japan, edited by K. Kajimura and H. Hayakawa (Springer-Verlag, Tokyo, 1991), pp. 337–342.
[12]H. Takagi, R. J. Cava, M. Marezio, B. Battlog, J. J. Krajewski, and W. F. Peck, Jr., Phys. Rev. Lett. **68**, 3777 (1992).
[13]K. Kitazawa, T. Nagano, Y. Nakayama, T. Tomioka, and K. Kishio, Appl. Supercond. **1**, 567 (1993).
[14]T. Nagano, Y. Tomioka, Y. Nakayama, K. Kishio, and K. Kitazawa, Phys. Rev. B **48**, 9689 (1993).
[15]N. Yamada and M. Ido, Physica C **203**, 240 (1992).
[16]R. J. Hill and C. J. Howard, *LHRL Report* (1987).
[17]D. B. Wiles and R. A. Young, J. Appl. Cryst. **14**, 149 (1981).
[18]J. D. Jorgensen, J. Faber, Jr., J. M. Carpenter, R. K. Crawford, J. R. Haumann, R. L. Hitterman, R. Kleb, G. E. Ostrowski, F. J. Rotella, and T. G. Worlton, J. Appl. Cryst. **22**, 321 (1989).
[19]R. B. von Dreele, J. D. Jorgensen, and C. J. Windsor, J. Appl. Cryst. **15**, 581 (1982).
[20]K. Ghiron, M. B. Salamon, B. W. Veal, A. P. Paulikas, and J. W. Downey, Phys. Rev. B **46**, 5837 (1992).
[21]A. R. Moodenbaugh, Y. Xu, M. Suenaga, T. J. Folkers, and R. J. Shelton, Phys. Rev. B **38**, 4596 (1988).
[22]J. D. Axe, A. H. Moudden, D. Hohlwein, D. E. Cox, K. M. Mohanty, A. R. Moodenbaugh, and Y. Xu, Phys. Rev. Lett. **62**, 2751 (1989).
[23]T. Fukase, T. Nomoto, T. Hanaguri, T. Goto, and Y. Koike, Physica B **165&166**, 1289 (1990).
[24]J. B. Goodenough and A. Manthiram, J. Solid State Chem. **88**, 115 (1990).
[25]R. D. Shannon, Acta Crystallogr. A **32**, 751 (1976).
[26]D. M. Hatch, H. T. Stokes, K. S. Aleksandrov, and S. V. Misyul, Phys. Rev. B **39**, 9282 (1989).
[27]D. Sahu and T. F. George, Solid State Commun. **65**, 1371 (1988).
[28]W. Ting, K. Fossheim, and T. Laegreid, Solid State Commun. **80**, 47 (1991).
[29]J. D. Axe, in *Lattice Effects in High-T_c Superconductors,* edited by Y. Bar-Yam, T. Egami, J. Mustre-de Leon, and A. R. Bishop (World Scientific, Singapore, 1992), pp. 517–530.
[30]H. T. Stokes and D. M. Hatch, *Isotropy Subgroups of the 230 Crystallographic Space Groups* (World Scientific, Singapore, 1988).
[31]K. Yoshimura, H. Kubota, H. Tanaka, Y. Date, M. Nakanishi, T. Ohmura, N. Saga, T. Sawamura, and T. Uemura, J. Phys. Soc. Jpn. **62**, 1114 (1993).